

# M-Channel Gating and Simulation

A. A. Selyanko and D. A. Brown

Department of Pharmacology, University College London, London WC1E 6BT, England

**ABSTRACT** Single potassium M-channels in rat sympathetic neurons have multiple voltage-dependent kinetic components in their activity: short, medium, and long closed times ( $\tau_{CS}$ ,  $\tau_{CM}$ , and  $\tau_{CL}$ ) and short and long open times ( $\tau_{OS}$  and  $\tau_{OL}$ ). All five components can be detected in cell-attached patches, but only four of them ( $\tau_{CS}$ ,  $\tau_{CM}$ ,  $\tau_{OS}$ , and  $\tau_{OL}$ ) in excised patches (Selyanko and Brown, 1993, *J. Physiol. (Lond.)* 472:711–724; 1996, *Neuron* 16:151–162; 1996, *Neuropharmacology* 35:933–947). Analysis of the burst structure of activity recorded from cell-attached and excised inside-out patches showed it to be consistent with the sequential kinetic scheme  $C_L \leftrightarrow O_S \leftrightarrow C_M \leftrightarrow O_L \leftrightarrow C_S$ . Using this scheme and experimentally determined kinetic parameters, we successfully simulated the activity of M-channels both under steady-state conditions and during depolarizing voltage steps. Consistent with the characteristic behavior of macroscopic M-current, ensemble currents constructed from simulated M-channels had exponential activation and deactivation, with no delays, when tested in the range between  $-50$  and  $-20$  mV.

## INTRODUCTION

M-current is a low-threshold, voltage-dependent, noninactivating  $K^+$  current that is inhibited by muscarinic stimulants (Brown and Adams, 1980). In response to step depolarization the current exhibits exponential activation, which contrasts with the sigmoidal activation of the delayed rectifier current (see Brown, 1988). This indicates that, although several closed and open voltage-dependent states can be detected in the activity of single M-channels (Selyanko and Brown, 1993), the gating scheme for the M-channel is probably different from that for the delayed rectifier channels, where the delay in activation is determined by the presence of several adjacent closed states (Zagotta et al., 1994; Klemic et al., 1998).

The aim of this work was to find a model that was capable of describing single-channel and macroscopic M-current kinetic behavior. To do so, we 1) analyzed the structure of steady-state M-channel activity, 2) determined a kinetic scheme consistent with it, 3) simulated steady-state M-channel activity at different membrane potentials, and 4) reconstructed the time-dependent activation and deactivation of the macroscopic M-current on the basis of steady-state M-channel activity simulated at two different membrane potentials.

## MATERIALS AND METHODS

Superior cervical ganglion neurons were dissociated from 15-day-old rats and cultured for 1–3 days. Single-channel experiments and analysis were performed as described previously (Selyanko and Brown, 1993, 1996a).

External (bath and intrapipette) solutions had the following composition (in mM): 144 NaCl; 2.5 KCl; 2 CaCl<sub>2</sub>; 0.5 MgCl<sub>2</sub>; 5 HEPES; 10 glucose

(pH 7.4 with Tris base). Nominally  $Ca^{2+}$ -free external solution contained no added  $Ca^{2+}$  and elevated (6 mM)  $Mg^{2+}$ . Membrane patches were excised into the following internal solution (mM): 175 KCl; 5 HEPES; 1 1,2-bis(2-aminophenoxy)ethane-*N,N,N,N*-tetraacetic acid (pH 7.2 with NaOH).

Whole-cell recordings were made in amphotericin B-perforated patch mode (Rae et al., 1991), with the use of the following internal (intrapipette) solution (mM): 90 K acetate; 20 KCl; 40 HEPES; 3 MgCl<sub>2</sub>; 3 EGTA; 1 CaCl<sub>2</sub> (pH 7.4 with KOH) (Selyanko et al., 1992). M-currents were activated by stepping from  $-50$  to  $-30$  mV. Leak currents were recorded in response to a voltage step from  $-90$  to  $-70$  mV and subtracted from the M-current records. Whole-cell currents were sampled at 2 kHz and filtered at 500 Hz.

Single-channel records were sampled at 4.46 kHz and filtered at 500 Hz (at  $V_m = -50$  to 0 mV) or 250 Hz (at  $V_m = -70$  to  $-60$  mV).

Pipette resistance was 2–3 M $\Omega$  in whole-cell and  $\sim 10$  M $\Omega$  in single-channel experiments.

In cell-attached experiments the resting membrane potential level was assumed to be  $-60$  mV, in both control and  $Ca^{2+}$ -free bath solutions. (When measured on breakthrough in whole-cell mode, the resting potentials in 2 and 0 mM  $Ca^{2+}$  in the bath were not different, being  $-58.1 \pm 7.3$  mV and  $-62.0 \pm 6.8$  mV, respectively (Selyanko and Brown, 1996b).)

Individual M channels studied in this work had conductances of either  $\approx 7$  or  $\approx 11$  pS (Selyanko et al., 1992; Selyanko and Brown, 1993). Apart from conductance, the other properties of 7-pS and 11-pS channels (sensitivity to muscarine,  $Ca^{2+}$  and membrane potential, kinetics) seem to be similar.

Channel activity was simulated using the CSIM program (version 2.0; Axon Instruments, Foster City, CA), and both observed and simulated activities were analyzed using the pClamp version 6.0.3 (Axon Instruments). Simulated activities were obtained with the same resolution (sampling: 4.46 kHz; filtering: 500 Hz at  $\geq -50$  mV) as the observed ones. Observed and simulated records were analyzed in the same way. Channel open and closed states were identified on the basis of crossing the 50% level of the channel amplitude. Channel openings and closings shorter than 1 ms were ignored. Distributions of open and closed times were logarithmically binned and were fitted with exponential components by the method of maximum likelihood (see Colquhoun and Sigworth, 1995). The number of exponential densities used for fitting the histograms was determined in pStat on the basis of examination of the F-statistic ( $p > 0.99$ ). Only events that were greater than or equal to 1.5 ms were included in the fitted range. Open-point amplitude histograms were fitted with Gaussian curves. Bursts were defined as series of openings separated by long ( $\tau_{CL}$ ) closed times. The critical time ( $t_{crit}$ , the lower limit for gaps between the bursts) was calculated according to the criterion minimizing the total number of misclassified intervals (Jackson et al., 1983; Colquhoun and Sigworth, 1995),

Received for publication 25 August 1998 and in final form 19 May 1999.

Address reprint requests to Dr. A. A. Selyanko, Department of Pharmacology, University College London, Gower Street, London WC1E 6BT, England. Tel.: +44-171-419-3221; Fax: +44-171-380-7298; E-mail: a.selyanko@ucl.ac.uk.

© 1999 by the Biophysical Society

0006-3495/99/08/701/13 \$2.00

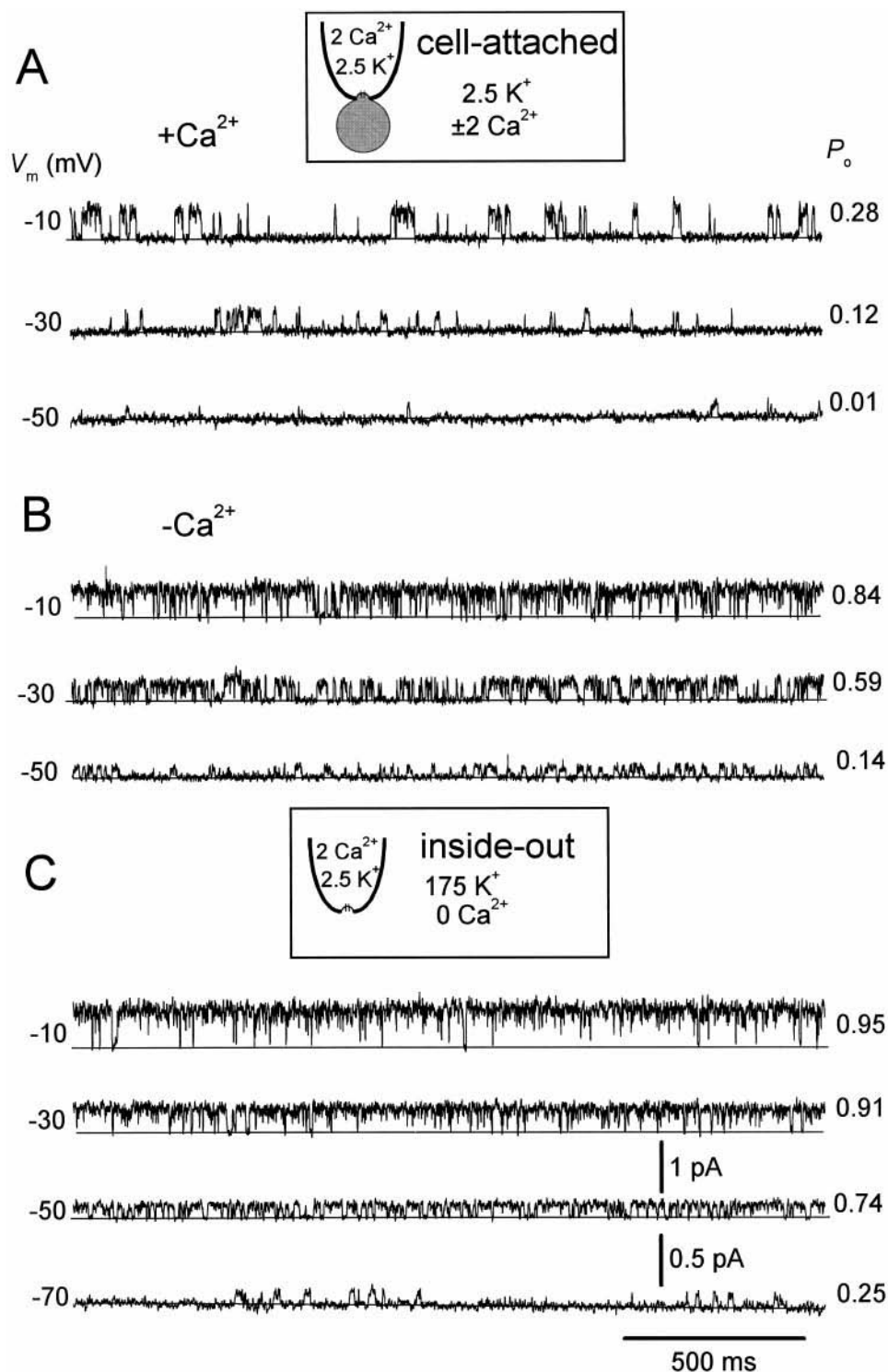


FIGURE 1 Steady-state activation of single M-channels by continuous membrane depolarization (experiment). Examples of single M-channel activity recorded at different membrane potentials (indicated in mV near each record, *left*) in cell-attached (*A*, *B*) and inside-out (*C*) modes. Note that the activity was strongly facilitated by membrane depolarization ( $P_o$  is indicated near each record, *right*). At all potentials tested the activity was low in control solution (*A*;  $[\text{Ca}^{2+}]_{\text{bath}} = 2 \text{ mM}$ ), but it increased when  $\text{Ca}^{2+}$  was omitted from the bath solution (*B*) or after the patch was excised into a  $\text{Ca}^{2+}$ -free internal solution (*C*). Data in *A*, *B*, and *C* were obtained from three different patches. Open point amplitude histograms (not shown) were fitted with single Gaussians, and the slope conductances (measured in the range between  $-50$  and  $-20 \text{ mV}$ ) were  $11.0$ ,  $7.1$ , and  $8.8 \text{ pS}$  in *A*, *B*, and *C*, respectively. Note that the bottom record in *C* is shown at the higher gain.

using the program EKDIST (D. Colquhoun, University College London; <http://www.ucl.ac.uk/Pharmacology/dc.html>).

The rate constants for simulation were chosen to reproduce the observed open and closed times and their areas according to the general rule that the lifetime of a state is given by  $1/(\text{sum of leaving rates})$ . When macrokinetics in response to voltage steps were simulated, the starting state at each potential was calculated according to the steady-state probability of occupancy at the preceding potential.

In each simulated record a background noise was introduced with an rms amplitude equal to that in the observed record. However, the observed open-channel noise was always higher than the closed-channel noise, and it increased with membrane depolarization—this has not been included in the simulation.

Linear and Boltzmann fits and all of the illustrations were constructed using the program Origin 5.0 (Microcal Software, Northampton, MA).

Significance levels were calculated using Student's *t*-test

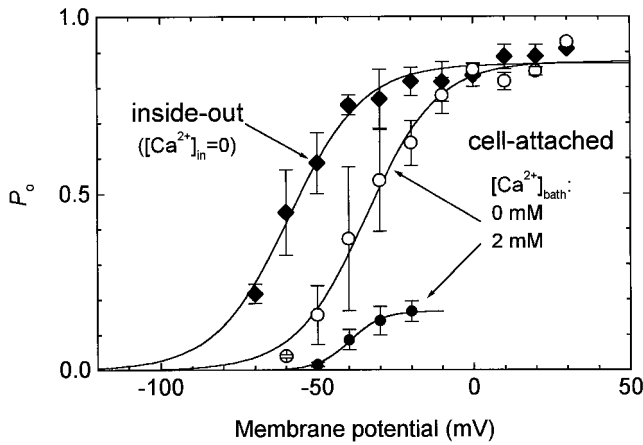


FIGURE 2 Voltage-dependent steady-state activation of single M-channels. Recordings were made in cell-attached mode, at  $[Ca^{2+}]_{bath} = 2$  mM (●) or 0 mM (○), and in inside-out mode, at  $[Ca^{2+}]_{in} = 0$  mM (◆). Mean data obtained from 13, 5, and 5 patches, respectively, are shown; vertical bars indicate SE of means. Activation curves were fitted by the Boltzmann equation (Eq. 1) at  $P_{o(max)}$ ,  $V_o$ , and  $a$  equal to  $0.17 \pm 0.01$ ,  $-39.8 \pm 1.3$  mV, and  $5.2 \pm 1.1$  mV (●);  $0.87 \pm 0.02$ ,  $-34.4 \pm 1.5$  mV, and  $11.3 \pm 1.3$  mV (○); and  $0.87 \pm 0.01$ ,  $-59.1 \pm 1.2$  mV, and  $11.8 \pm 1.3$  mV (◆).

## RESULTS

### Voltage-dependent activation of M-channels (experiment)

Fig. 1 shows examples of the steady-state M-channel activity recorded at different potentials in cell-attached (Fig. 1, A

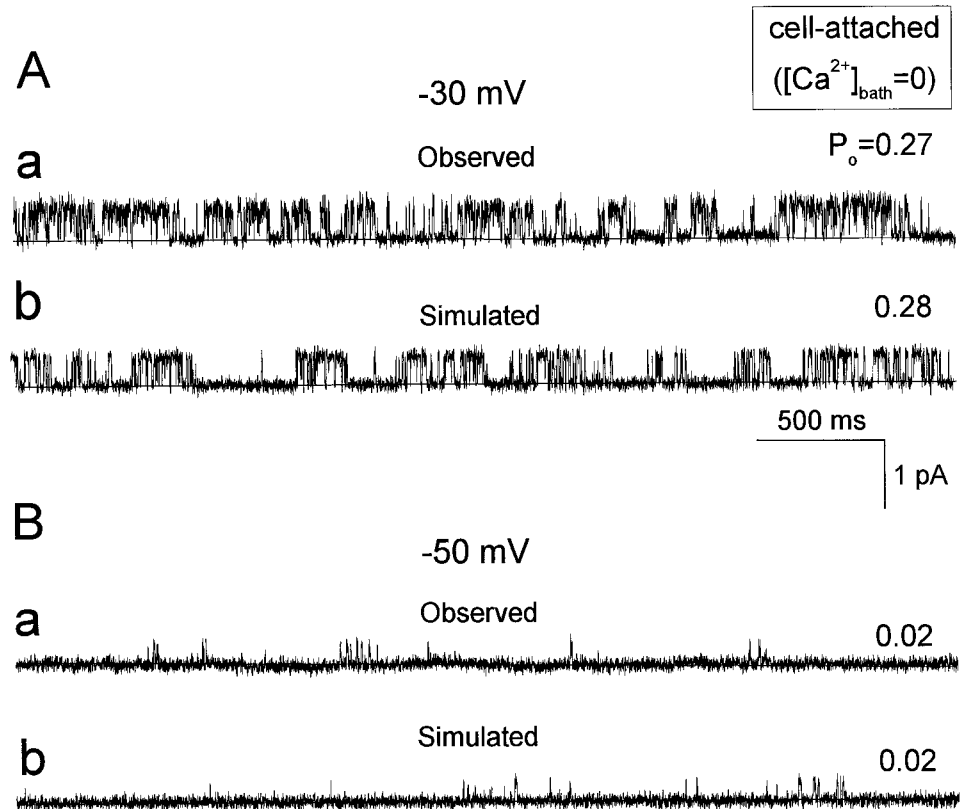
and B) and inside-out (Fig. 1 C) modes. The M-channels had a low threshold for activation, and their activity was markedly increased when  $Ca^{2+}$  was omitted from the extracellular (bath) solution or when the patch was excised into a  $Ca^{2+}$ -free internal solution (compare Fig. 1 A and Fig. 1, B and C; see also Selyanko and Brown, 1996a,b).

The mean steady-state activation of single M-channels recorded under different conditions was fitted by a Boltzmann equation (Fig. 2):

$$P_o/P_{o(max)} = 1/\{1 + \exp[(V_o - V_m)/a]\}, \quad (1)$$

where  $P_o$  is the channel open probability and  $P_{o(max)}$  is the maximum  $P_o$  attained at strongly depolarized membrane potentials;  $V_m$  is the assumed membrane potential (estimated as  $V_{rest} - V_{pipette}$ , where  $V_{rest} = -60$  mV; see Materials and Methods) and  $V_o$  is the half-activation potential, i.e., the potential where  $P_o = 1/2 P_{o(max)}$ ; and  $a$  is the slope factor that indicates the potential change required for an  $e$ -fold increase in  $P_o$ . In cell-attached mode the increase in M-channel activity produced by omitting  $Ca^{2+}$  from the bathing solution was accompanied by a significant rise in  $P_{o(max)}$ , from  $0.17 \pm 0.01$  ( $n = 13$ ) to  $0.87 \pm 0.02$  ( $n = 5$ ), and an increase in  $a$ , from  $5.2 \pm 1.1$  mV to  $11.3 \pm 1.3$  mV, with little change in  $V_o$  ( $-39.8 \pm 1.3$  mV and  $-34.4 \pm 1.5$  mV; see Fig. 2). Similar changes in the activation parameters were noted on excising patches into inside-out mode:  $P_{o(max)}$  increased to  $0.87 \pm 0.01$  ( $n = 5$ ), and  $a$  increased to  $11.8 \pm 1.3$  mV. In addition, there was a  $\sim 20$ -mV negative shift in  $V_o$  (to  $-59.1 \pm 1.2$  mV; Fig. 2).

FIGURE 3 M-channel activity recorded in cell-attached mode and its simulation. (A and B) Examples of the observed (a) and simulated (b) activities at  $-30$  mV (A) and  $-50$  mV (B). Activity was increased by a  $Ca^{2+}$ -free bath solution. It was simulated according to the scheme shown in Fig. 7 B. The rate constants used for simulation were  $k_{1-2} = 10$  s $^{-1}$ ;  $k_{2-1} = 100$  s $^{-1}$ ;  $k_{2-3} = 250$  s $^{-1}$ ;  $k_{3-2} = 50$  s $^{-1}$ ;  $k_{3-4} = 50$  s $^{-1}$ ;  $k_{4-3} = 50$  s $^{-1}$ ;  $k_{4-5} = 100$  s $^{-1}$ ;  $k_{5-4} = 670$  s $^{-1}$  at  $-30$  mV and  $k_{1-2} = 1.6$  s $^{-1}$ ;  $k_{2-1} = 300$  s $^{-1}$ ;  $k_{2-3} = 300$  s $^{-1}$ ;  $k_{3-2} = 14$  s $^{-1}$ ;  $k_{3-4} = 8$  s $^{-1}$ ;  $k_{4-3} = 50$  s $^{-1}$ ;  $k_{4-5} = 110$  s $^{-1}$ ;  $k_{5-4} = 220$  s $^{-1}$  at  $-30$  mV.



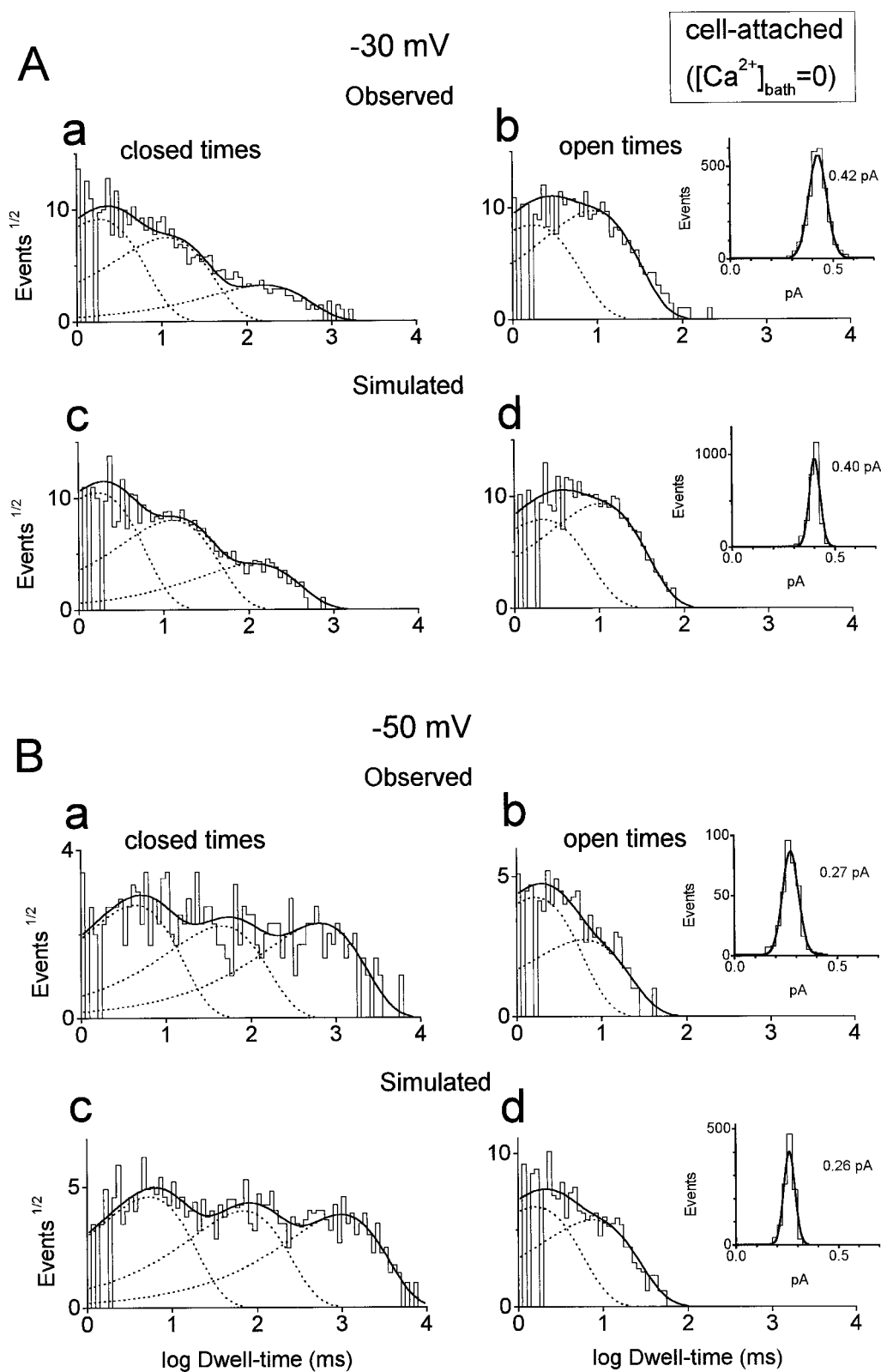


FIGURE 4 Kinetics of the observed and simulated M-channel activities shown in Fig. 3. Shown are closed (*a,c*) and open (*b,d*) time distributions for the observed (*a,b*) and simulated (*c,d*) channel activities at  $-30$  (*A*) and  $-50$  mV (*B*). Distributions were fitted by exponential densities. Individual components are shown by dotted lines and their sums by smooth lines. See Table 1 for the fitted parameters and the initial parameters of simulation. The recording time was 86.4 s (*Aa,b*), 86.7 s (*Ac,d*), and 383.3 s (*Ba,b* and *Ac,d*).

### Kinetic components and structure of the M-channel activity (experiment)

The kinetics of M-channel activity were first analyzed in cell-attached mode, under conditions where the channel activity was increased by a  $\text{Ca}^{2+}$ -free solution. This maintained channels in their “physiological” cytoplasmic environment, yet allowed the clear identification of single M-channels and yielded a sufficient number of events for analysis. At the same time, this increased activity, like the control activity, showed both sustained (see above) and time-dependent (data not shown) activations with membrane depolarization, all five kinetic components in the steady-state activity (see Selyanko and Brown, 1993, 1996b, and below), and similar burst structure (see below).

Fig. 3 shows examples of single-channel activity used for the analysis and simulation. The activity was recorded at two membrane potentials,  $-30$  mV (Fig. 3 *Aa*) and  $-50$  mV (Fig. 3 *Ba*). These were close to the half-activation and the threshold potentials, respectively. Fig. 4 shows that at both potentials the activity could be fitted with a mixture of three exponential densities in closed time distribution, with short ( $\tau_{\text{CS}}$ ), medium ( $\tau_{\text{CM}}$ ), and long ( $\tau_{\text{CL}}$ ) time constants (Fig. 4, *Aa* and *Ba*), and with a mixture of two exponential densities in open time distribution, with short ( $\tau_{\text{OS}}$ ) and long ( $\tau_{\text{OL}}$ ) time constants (Fig. 4, *Ab* and *Bb*). The closed time constants decreased with membrane depolarization, with an increase in the contributions of medium and long kinetic components (Fig. 4, *Aa* and *Ba*, and Table 1), whereas the open time constants lengthened with membrane depolarization, with an increase in the contribution of the longer

kinetic component (Fig. 4, *Ab* and *Bb*, and Table 1). The relationships between the kinetic components and membrane potential were monotonic and, when plotted semi-logarithmically, were fitted with straight lines (Fig. 5 *A*). Current amplitudes obtained at two potentials were fitted with single Gaussian distributions (see *insets* in Fig. 4, *Ab* and *Bb*), indicating that the channel had only one conductance level.

This kinetic behavior and its voltage dependence were in agreement with the previous data obtained with normal ( $2$  mM)  $\text{Ca}^{2+}$  in the bath (Selyanko and Brown, 1993).

The presence of five kinetic components in the activity suggests that there are five most stable states of the channel: short ( $\text{C}_\text{S}$ ), medium ( $\text{C}_\text{M}$ ), and long ( $\text{C}_\text{L}$ ) closed and short ( $\text{O}_\text{S}$ ) and long ( $\text{O}_\text{L}$ ) open. The sequence of these states in the activity was deduced from the analysis of the burst structure. Bursts were defined as multiple channel openings separated by long ( $\text{C}_\text{L}$ ) closed states. An example of burst analysis for the activity recorded at  $-30$  mV and illustrated in Fig. 3 *Aa* and Fig. 4 *Aa,b* is shown in Fig. 6 *A*. The distributions of closed times within a burst (shorter than  $t_{\text{crit}} = 53$  ms) were fitted with two exponential densities. However, in the distribution of all closed times in a burst, the short ( $\tau_{\text{CS}}$ ) component was predominant (area: 59.7%; Fig. 6 *Aa*, *medium line*), whereas in the distributions of the first (Fig. 6 *Aa*, *thick line*) and the last (Fig. 6 *Aa*<sub>1</sub>) closed times in a burst, the medium ( $\tau_{\text{CM}}$ ) component was predominant (areas for  $\tau_{\text{CM}}$ : 64.8% and 77.6%, respectively).

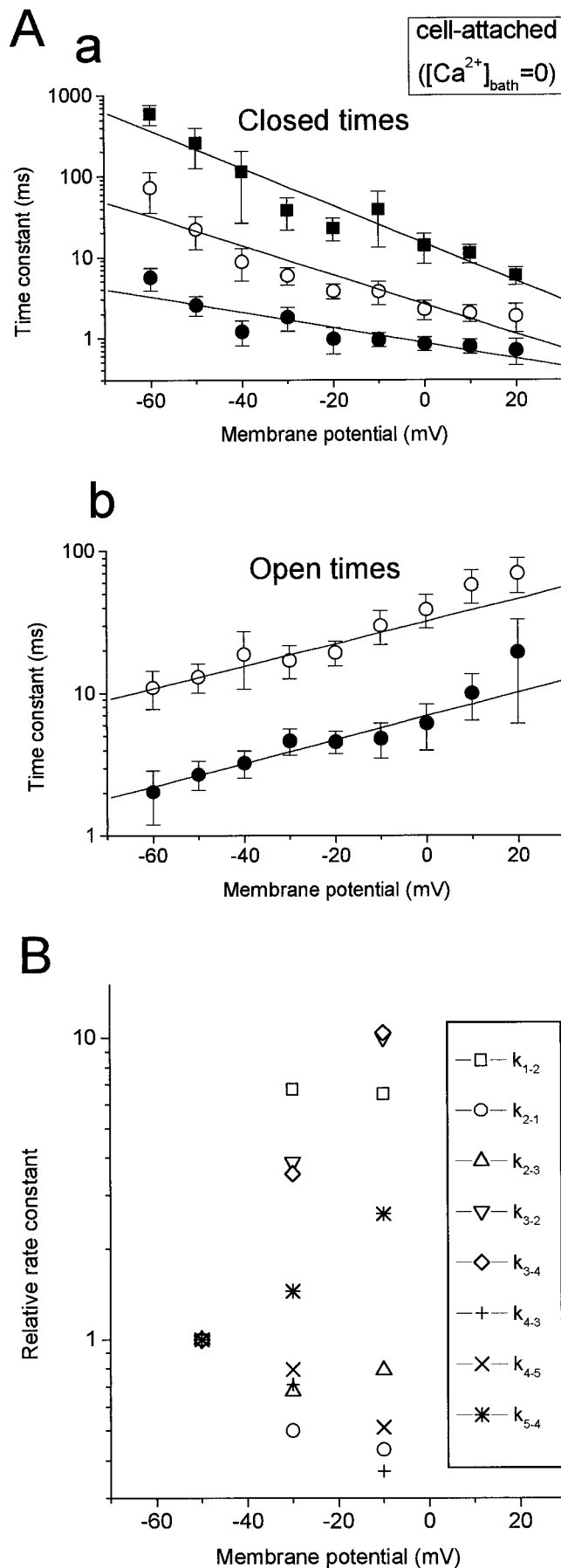
The distribution of open time intervals in a burst (Fig. 6 *Ab*, *medium line*) was similar to that of all open time

**TABLE 1** Fitted parameters of closed and open times and open point amplitude distributions for the observed and simulated activities shown in Fig. 4 (cell-attached patch;  $[\text{Ca}^{2+}]_{\text{bath}} = 0$  mM)

$\tau_{\text{CS}}$	$\tau_{\text{CM}}$	$\tau_{\text{CL}}$	$\tau_{\text{OS}}$	$\tau_{\text{OL}}$	$i$	SD
−30 mV						
Observed						
1.8 ms (55.5%)	11.5 ms (37.4%)	159 ms (7.1%)	1.8 ms (43.7%)	8.9 ms (56.3%)	0.42 pA	0.09 pA
Simulated						
Fitted parameters						
1.7 ms (56.2%)	12.7 ms (34.8%)	115 ms (8.9%)	2.2 ms (41.7%)	10.4 ms (58.3%)	0.40 pA	0.05 pA
Initial parameters						
1.5 ms	10 ms	100 ms	2.8 ms	6.7 ms	0.42 pA	
−50 mV						
Observed						
4.4 ms (42.6%)	45.2 ms (27.9%)	642 ms (29.5%)	1.7 ms (70.4%)	6.2 ms (29.6%)	0.27 pA	0.08 pA
Simulated						
Fitted parameters						
5.4 ms (40.2%)	69.2 ms (30.6%)	982 ms (29.1%)	1.6 ms (57.1%)	7.6 ms (42.9%)	0.26 pA	0.05 pA
Initial parameters						
4.5 ms	45 ms	625 ms	1.7 ms	6.3 ms	0.27 pA	

Numbers in brackets indicate areas under the fitted components;  $i$  is the current amplitude, and SD is its standard deviation obtained from the Gaussian fit (in the initial parameters rms amplitude for the background noise was set at 0.1 pA). The initial parameters for simulation were taken close to the experimental ones, and the relationships between the initial time constants and the rate constants in the scheme shown in Fig. 7 *B* were  $\tau_{\text{CS}} = 1/k_{5-4}$ ;  $\tau_{\text{CM}} = 1/(k_{3-2} + k_{3-4})$ ;  $\tau_{\text{CL}} = 1/k_{1-2}$ ;  $\tau_{\text{OS}} = 1/(k_{2-3} + k_{2-1})$ ;  $\tau_{\text{OL}} = 1/(k_{4-5} + k_{4-3})$ .





intervals (Fig. 6 *Ab*, *thin line*), and it was fitted with two exponential densities with a predominately long ( $\tau_{OS}$ ) component (area: 56.3%; Fig. 6 *Ba*, *medium line*). At the same time, the distributions of durations of the first (Fig. 6 *Ab*, *thick line*) and the last (Fig. 6 *Ab*<sub>1</sub>) openings within a burst were fitted with two exponential densities with a predominately short ( $\tau_{OS}$ ) component (areas: 70.1% and 68.8%, respectively).

As determined in four patches under the same conditions, the mean area under the medium closed time component ( $\tau_{CM}$ ) was significantly ( $p < 0.01$ ) smaller for all closed times in a burst ( $30.9 \pm 2.9\%$ ) than for the last ( $70.9 \pm 3.0\%$ ) or the first ( $73.3 \pm 4.0\%$ ) closed times in a burst. The mean area under the long open time component ( $\tau_{OL}$ ) was significantly ( $p < 0.01$ ) higher for all open times in a burst ( $67.9 \pm 5.6\%$ ) than for the last ( $23.8 \pm 3.7\%$ ) or the first ( $21.4 \pm 4.0\%$ ) open times in a burst.

In the presence of 2 mM Ca<sup>2+</sup> in the bath, a similar difference was found between all closed/open times and the first and the last closed/open times in a burst (two patches).

### Kinetic scheme

The results of the burst analysis showed that the long (interburst) closed states ( $C_L$ ) are adjacent to the short open states ( $O_S$ , first and last open states within the burst), which, in turn, are adjacent to the medium closed states ( $C_M$ , first and last closed states within the burst). Furthermore, in the activity recorded from inside-out patches long (interburst) closed states ( $C_L$ ) were missing (see below). This sequence of states in the activity is represented by a schematic diagram illustrated in Fig. 7 *A* and is most consistent with the simple sequential kinetic scheme where three closed states are separated by two open states (Fig. 7 *B*).

### Simulation of the M-channel activity

On the basis of this kinetic scheme and kinetic components obtained from closed and open time distributions, the sum

**FIGURE 5** Voltage dependence of the M-channel gating. (*A*) Mean closed (*a*) and open (*b*) time components (vertical lines, SE means) plotted against membrane potential. (*Aa*) Short ( $\tau_{CS}$ , filled circles), medium ( $\tau_{CM}$ , open circles) and long ( $\tau_{CL}$ , squares) closed time components. (*Ab*) Short ( $\tau_{OS}$ , closed circles) and long ( $\tau_{OL}$ , open circles) open time components. Kinetic components were plotted semilogarithmically, and  $\tau$ - $V$  relationships were fitted by straight lines. Values for  $\tau$  at 0 mV were  $0.9 \pm 1.2$  ms ( $\tau_{CS}$ ),  $2.6 \pm 1.2$  ms ( $\tau_{CM}$ ), and  $14.8 \pm 1.2$  ms ( $\tau_{CL}$ ) in *a*, and  $1.0 \pm 1.1$  ms ( $\tau_{OS}$ ) and  $39.8 \pm 1.1$  ms ( $\tau_{OL}$ ) in *b*. Values for the slope were  $-0.0095 \pm 0.0019$  mV<sup>-1</sup> ( $\tau_{CS}$ ),  $-0.018 \pm 0.0027$  mV<sup>-1</sup> ( $\tau_{CM}$ ), and  $-0.023 \pm 0.0025$  mV<sup>-1</sup> ( $\tau_{CL}$ ) in *a* and  $0.01 \pm 0.001$  mV<sup>-1</sup> ( $\tau_{OS}$ ) and  $0.01 \pm 0.0001$  mV<sup>-1</sup> ( $\tau_{OL}$ ) in *b*. The data were obtained in cell-attached mode from five patches in the absence of Ca<sup>2+</sup> in the bath. (*B*) Rate constants (normalized to those at -50 mV) plotted semilogarithmically against membrane potential. The rate constants were obtained from simulation of the activity at three membrane potentials on the basis of a five-state kinetic scheme (Fig. 7 *B*) and kinetic components shown in *A*. For the absolute values of the rate constants at -50 mV and -30 mV, see Table 2.

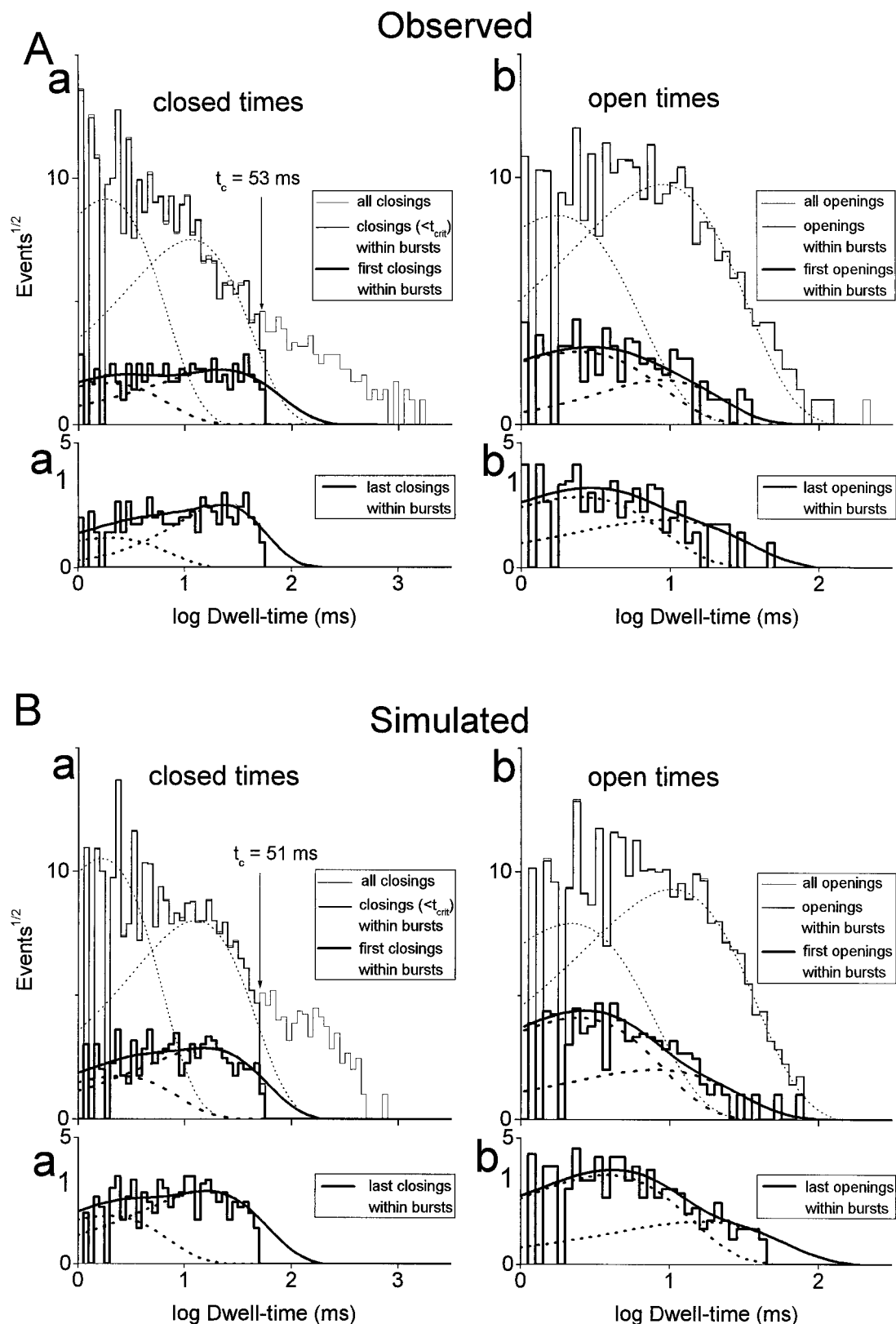
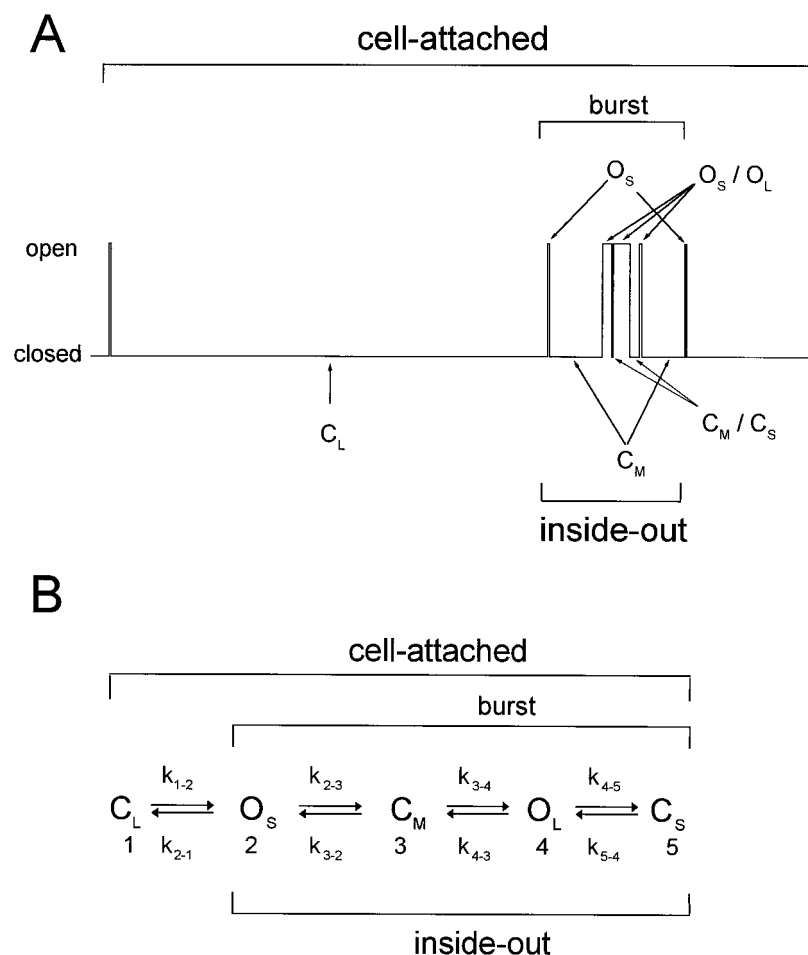


FIGURE 6 Analysis of burst structure for the observed (*A*) and simulated (*B*) activities illustrated in Figs. 3 *A* and 4 *A*. Distributions of closed (*a*) and open (*b*) times are shown for all of the events in the activity (*thin lines*), all of the events within the burst (*medium lines*), and the first events within the burst (*thick lines*). Distributions of the last closed and open times are shown in *a<sub>1</sub>* and *b<sub>1</sub>*. The critical times ( $t_{crit}$ ), calculated as specified in Materials and Methods, were 53 ms (*A*) and 51 ms (*B*) (indicated by arrows), and the total number (out of 100) of events that were misclassified was 5.4 in *A* and 3.8 in *B*. The number of bursts, the mean burst length, the mean total open time per burst, and the mean number of openings per burst were 197, 212 ms, 125 ms, and 14.1 in *A* and 273, 171.7 ms, 104.7 ms, and 10.5 in *B*. In the closed time distributions for the observed activity the fitted curves were  $\tau_{CS} = 1.8$  ms.

FIGURE 7 Schematic representation of the M-channel activity (*A*) and the kinetic scheme (*B*).  $C_S$ ,  $C_M$ , and  $C_L$  are short, medium, and long closed and  $O_S$  and  $O_L$  are short and long open channel states. All states were present in cell-attached mode, whereas the long closed state,  $C_L$ , was absent in inside-out mode. The burst defined as a series of openings separated by the long closed state,  $C_L$ , contained two open ( $O_S$  and  $O_L$ ) and two closed ( $C_S$  and  $C_M$ ) states, of which  $O_S$  and  $C_M$  were the first/last open and closed states within a burst. Note that all closed states were separated by the open ones.



of leaving rate constants was calculated for each state as described in Materials and Methods. By keeping the sums constant and adjusting the individual rate constants, many runs of simulation and analysis were required to produce the record with the kinetic components (time constants and areas) similar to those in the observed activity. Examples of simulation of the steady-state M-channel activity at two different membrane potentials,  $-30$  mV and  $-50$  mV, are shown in Fig. 3, *Ab* and *Bb*. Simulated activities had distributions of closed (Fig. 4, *Ac* and *Bc*, and Table 1) and open (Fig. 4, *Ad* and *Bd*, and Table 1) times, fitted parameters, and burst structure (Fig. 6 *B*) very similar to those for the observed activity. Furthermore, the fitted parameters for simulated activity were very close to the initial parameters for simulation (see Table 1). All of this suggests that

both the kinetic scheme and the methods of data acquisition and analysis employed in these experiments were adequate. Under the same conditions similar results were obtained from three other patches studied.

In patches excised into a  $Ca^{2+}$ -free internal solution, an increase in the M-channel activity was accompanied by the loss of its long ( $\tau_{CL}$ ) closed time component (see also Selyanko and Brown, 1996b). Fig. 8 *Aa* shows an example of high-rate activity of a single M-channel recorded at  $-20$  mV that had only two components in its closed time distribution (Fig. 8 *Ba*) and the usual two components in the open time distribution (Fig. 8 *Bb*). The activity of M-channels recorded from excised patches was therefore simulated on the basis of the same main scheme, but contained a reduced number of closed states. Fig. 8 *Ab* shows the result of

(59.7%) and  $\tau_{CM} = 11.5$  ms (40.3%) for all of the closed times (*Aa*, medium lines),  $\tau_{CS} = 1.7$  ms (35.2%) and  $\tau_{CM} = 19.5$  ms (64.8%) for the first closed times (*Aa*, thick lines), and  $\tau_{CS} = 1.9$  ms (22.4%) and  $\tau_{CM} = 21.5$  ms (77.6%) for the last closed times (*Aa*) in a burst. In the closed time distributions for the simulated activity, the fitted curves were  $\tau_{CS} = 1.7$  ms (61.8%) and  $\tau_{CM} = 12.7$  ms (38.2%) for all of the closed times (*Ba*, medium lines),  $\tau_{CS} = 2.2$  ms (27.2%) and  $\tau_{CM} = 14.5$  ms (62.8%) for the first closed times (*Ba*, thick lines), and  $\tau_{CS} = 2.0$  ms (30.4%) and  $\tau_{CM} = 14.7$  ms (69.6%) for the last closed times (*Ba*) in a burst. In the open time distributions for the observed activity, the fitted curves were  $\tau_{OS} = 1.8$  ms (43.7%) and  $\tau_{OL} = 8.9$  ms (56.3%) for all of the open times (*Ab*, medium lines),  $\tau_{OS} = 2.5$  ms (70.1%) and  $\tau_{OL} = 9.0$  ms (29.9%) for the first open times (*Ab*, thick lines), and  $\tau_{OS} = 2.2$  ms (68.8%) and  $\tau_{OL} = 8.3$  ms (31.2%) for the last open times (*Ab*) in a burst. In the open time distributions for the simulated activity, the fitted curves were  $\tau_{OS} = 2.2$  ms (41.7%) and  $\tau_{OL} = 10.4$  ms (58.3%) for all of the open times (*Ab*, medium lines),  $\tau_{OS} = 2.5$  ms (80.6%) and  $\tau_{OL} = 8.1$  ms (19.4%) for the first open times (*Ab*, thick lines), and  $\tau_{OS} = 3.4$  ms (81.2%) and  $\tau_{OL} = 14.5$  ms (18.8%) for the last open times (*Ab*) in a burst.



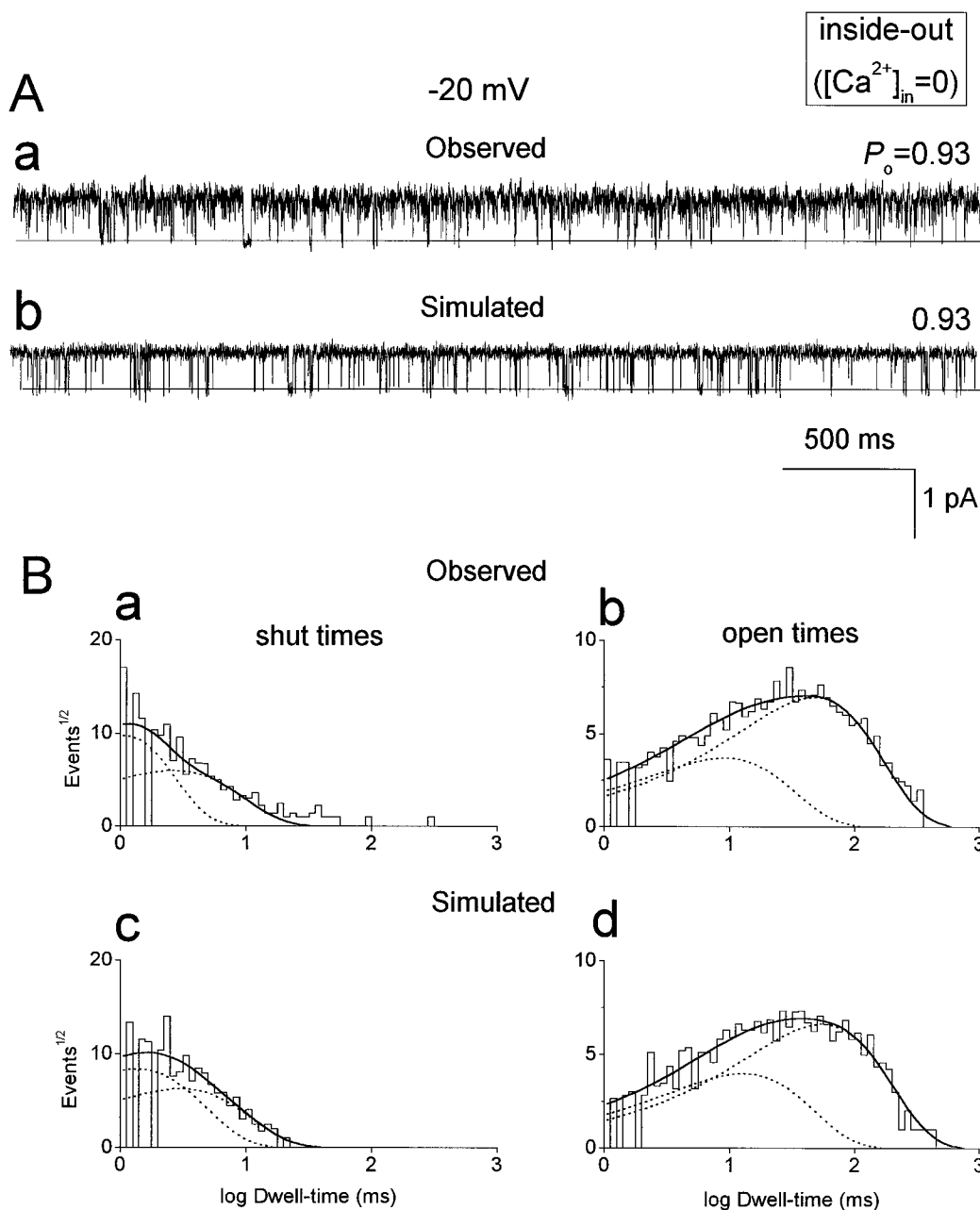


FIGURE 8 M-channel activity recorded in inside-out mode and its simulation. (A) Examples of the observed (a) and simulated (b) activities (at  $-20$  mV). (B) Distributions of closed (a,c) and open (b,d) times for the observed (a,b) and simulated (c,d) activities fitted by exponential densities. Individual components of the fit and their sums are shown by dotted and smooth lines, respectively. The parameters of the fit were  $\tau_{CS} = 1.0$  ms (72.4%) and  $\tau_{CM} = 2.7$  ms (27.6%) in a;  $\tau_{OS} = 9.1$  ms (21.3%) and  $\tau_{OL} = 46.9$  ms (78.7%) in b;  $\tau_{CS} = 1.3$  ms (64.1%) and  $\tau_{CM} = 3.0$  ms (35.9%) in c; and  $\tau_{OS} = 12.8$  ms (27.0%) and  $\tau_{OL} = 54.9$  ms (73.0%) in d. Recording time: 64.0 s in the observed and 65.4 s in simulated activities. The activity in Ab was simulated according to the four-state scheme shown in Fig. 7 B. The rate constants used for simulation were  $k_{2-3} = 200$  s<sup>-1</sup>;  $k_{3-2} = 200$  s<sup>-1</sup>;  $k_{3-4} = 80$  s<sup>-1</sup>;  $k_{4-3} = 11$  s<sup>-1</sup>;  $k_{4-5} = 4$  s<sup>-1</sup>;  $k_{5-4} = 1000$  s<sup>-1</sup>.

simulating activity on the basis of a four-state variant of the kinetic scheme (Fig. 7 B); distributions of closed (Fig. 8 Bc) and open (Fig. 8 Bd) times and their fitted components were similar to those for the observed activity. Activity could be simulated using the same four-state scheme in three other patches studied under the same conditions.

Table 2 presents the mean kinetic components in the activities recorded at  $-50$  and  $-30$  mV in cell-attached

mode, with 0 and 2 mM  $Ca^{2+}$  in the bath, and in inside-out mode, in the absence of  $Ca^{2+}$  in the internal solution, and the rate constants obtained from simulation with these components. The removal of  $Ca^{2+}$  from the bath resulted in strong acceleration of all rate constants, and some of them increased further on patch excision. Moreover, as expected from the voltage dependence of kinetic components (Fig. 5 A) and predicted by the scheme (Fig. 7 B), the leaving rate

**TABLE 2** Mean kinetic components in the M-channel activity and the rate constants obtained from their simulation

	-30 mV			-50 mV		
	Cell-attached: $[Ca^{2+}]_{bath}$ (mM)			Cell-attached: $[Ca^{2+}]_{bath}$ (mM)		
	2*	0	Inside-out	2*	0	Inside-out
Time constant (ms)						
(area, %)						
$\tau_{CS}$	8.0 $\pm$ 2.2 (43.6 $\pm$ 6.0)	1.8 $\pm$ 1.3 (51.6 $\pm$ 19.8)	0.8 $\pm$ 0.5 (67.4 $\pm$ 37.9)	7.4 $\pm$ 1.5 (35.5 $\pm$ 5.5)	2.6 $\pm$ 1.4 (34.9 $\pm$ 25.4)	1.8 $\pm$ 1.5 (65.2 $\pm$ 12.8)
$\tau_{CM}$	71.3 $\pm$ 8.6 (27.6 $\pm$ 5.8)	5.9 $\pm$ 3.3 (38.2 $\pm$ 13.5)	3.8 $\pm$ 1.3 (15.7 $\pm$ 5.0)	293 $\pm$ 78.1 (30.2 $\pm$ 8.5)	22.1 $\pm$ 19.2 (46.9 $\pm$ 29.8)	6.5 $\pm$ 1.3 (34.8 $\pm$ 12.8)
$\tau_{CL}$	740 $\pm$ 220 (28.2 $\pm$ 8.1)	37.6 $\pm$ 36.0 (10.2 $\pm$ 6.4)	—	1857 $\pm$ 657 (32.9 $\pm$ 9.5)	258 $\pm$ 267 (18.2 $\pm$ 9.6)	—
$\tau_{OS}$	10.6 $\pm$ 1.9 (73.9 $\pm$ 4.7)	4.6 $\pm$ 2.1 (36.5 $\pm$ 19.8)	8.4 $\pm$ 5.5 (32.5 $\pm$ 46.1)	3.8 $\pm$ 0.7 (82.5 $\pm$ 9.1)	2.7 $\pm$ 1.2 (56.1 $\pm$ 13.4)	3.9 $\pm$ 5.0 (36.4 $\pm$ 41.4)
$\tau_{OL}$	59.3 $\pm$ 8.7 (26.0 $\pm$ 4.7)	17.0 $\pm$ 10.1 (63.5 $\pm$ 19.5)	30.5 $\pm$ 13.2 (54.0 $\pm$ 45.1)	17.8 $\pm$ 4.5 (17.4 $\pm$ 9.1)	13.0 $\pm$ 6.1 (43.9 $\pm$ 13.1)	9.2 $\pm$ 3.7 (63.6 $\pm$ 40.0)
<i>n</i>	10	5	5	10	5	5
Rate constant ( $s^{-1}$ )						
$k_{1-2}$	1.4	27	—	0.54	4	—
$k_{2-1}$	40	90	—	150	180	—
$k_{2-3}$	60	128	120	110	190	256
$k_{3-2}$	10	85	140	2.5	22	80
$k_{3-4}$	4	85	123	0.9	24	74
$k_{4-3}$	5	27	13	28	38	60
$k_{4-5}$	11	31	20	28	39	47
$k_{5-4}$	130	556	1250	140	385	556

Means  $\pm$  SE of means. Areas are in brackets. *n* = number of patches. \*Time constants from Selyanko and Brown (1993).

constants for the closed states ( $k_{1-2}$ ,  $k_{3-2}$ ,  $k_{3-4}$ , and  $k_{5-4}$ ) were increased, whereas those for the open states ( $k_{2-1}$ ,  $k_{2-3}$ ,  $k_{4-3}$ , and  $k_{4-5}$ ) were decreased by membrane depolarization (Fig. 5 B).

### Reconstruction of the macroscopic M-current

The macroscopic M-current exhibits its distinctive voltage- and time-dependent properties in response to the standard "M-current voltage protocol" (Brown, 1988), comprising 1-s steps between the levels close to its threshold and half-activation ( $-50$  and  $-30$  mV, respectively). As a result, during the voltage step the M-current shows an instantaneous ("ohmic") change, due to the change in e.m.f. for the current, followed by an exponential growth (at  $-30$  mV) and decay (at  $-50$  mV). Thus the voltage- and time-dependent activation of M-channels was reproduced by simulating a steady-state multichannel activity at  $-50$  mV and introducing a sudden, 1-s-long change in the rate constants, from those at  $-50$  to those at  $-30$  mV. The rate constants were obtained by simulating steady-state single-channel activities at  $-50$  and  $-30$  mV, on the basis of the kinetic components previously reported at these potentials in normal ( $[Ca^{2+}]_{bath} = 2$  mM) conditions (Table 2; see also Selyanko and Brown, 1993). As a result, a time-dependent ensemble current was generated (Fig. 9 Aa), and the summing of many such responses produced a curve (Fig. 9 Ab) approximately matching the observed macroscopic M-current (Fig. 9 B).

### Modal gating?

Recent kinetic analysis of M-channels in bullfrog sympathetic neurons indicated that they have two modes of gating, with a short open time and low  $P_o$  and a long open time and high  $P_o$ , respectively, and that both modes were voltage dependent and suppressed by intracellular  $Ca^{2+}$  (acting through channel-associated calcineurin), whereas only a high- $P_o$  mode was inhibited by muscarine (Marrion, 1993, 1996, 1997). Because M-channels in rat sympathetic neurons also have two open time components, runs analysis was performed for their observed activities to check whether they have two modes of  $P_o$ .

Fig. 10, Aa, Ba, and Ca, shows the results of runs analysis of M-channel activity recorded from a cell-attached patch at three different membrane potentials,  $-60$  mV (A),  $-40$  mV (B), and  $0$  mV (C), when the activity was increased by the use of  $Ca^{2+}$ -free bath solution. (Graphs in Fig. 10, Aa, Ba, and Ca, also represent stability plots (Weiss and Magleby, 1989) for  $P_o$  and illustrate the lack of M-channel inactivation.) It is obvious that there is only one peak in the distribution of  $P_o$ , close either to 0 (at  $-60$  mV, near the threshold for M-channel activation) or to 1 (at  $0$  mV, where the channel is fully activated) (Fig. 10, Bb and Cb). At the same time, during partial activation of the M-channel (at  $-40$  mV),  $P_o$  had a broad distribution, between 0 and 0.7, with no clear double peaks (Fig. 10 Bb). There was also a voltage-dependent relationship between the mean open time and  $P_o$ : in the example illustrated in Fig. 10, Ac, Bc, and Cc,

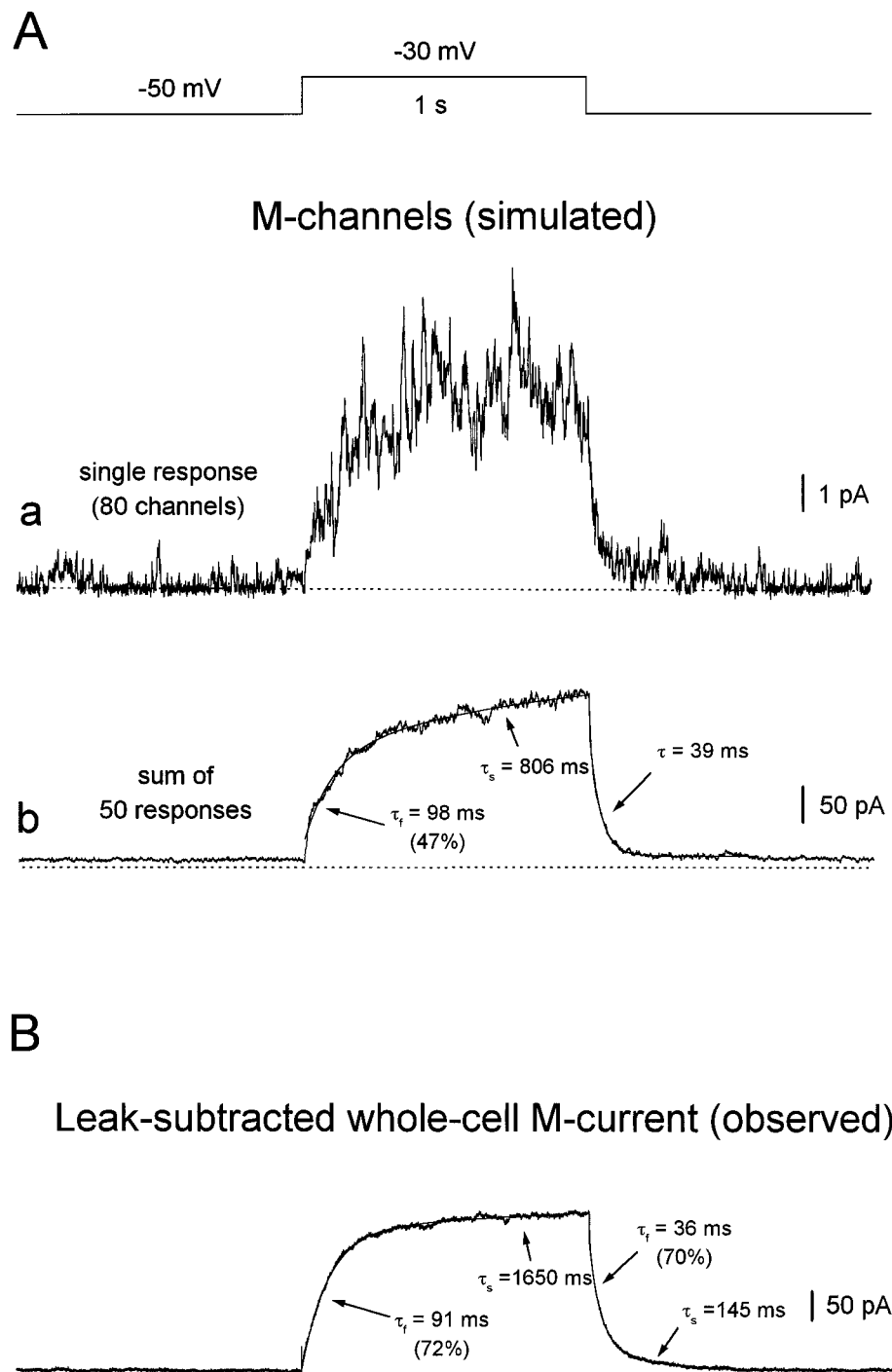


**FIGURE 9** Reconstruction of the macroscopic M-current on the basis of steady-state channel activity simulated at two different membrane potentials,  $-50$  and  $-30$  mV. Voltage- and time-dependent activation of macroscopic M-current (recorded in perforated patch whole-cell mode and exemplified in *B*) was reconstructed on the basis of multiple M-channel activity (*A*) simulated according to the five-state kinetic scheme (Fig. 7 *B*) at  $-50$  and  $-30$  mV. For simulation, average parameters used were those previously reported for steady-state activity recorded in cell-attached mode in the presence of  $2$  mM  $\text{Ca}^{2+}$  in the bath (see Selyanko and Brown, 1993). Average kinetic components and rate constants are shown in Table 2. In *B* the leak subtraction was obtained by subtracting the average of eight currents recorded in response to a voltage step from  $-90$  to  $-70$  mV from the average of eight currents recorded in response to a voltage step from  $-50$  to  $-30$  mV.

this relationship was insignificant at  $-60$  mV (*Ac*), but significant at  $-40$  (*Bc*) and  $0$  mV (*Cc*).

Overall, the modal gating was examined in the activities recorded in cell-attached mode in  $[\text{Ca}^{2+}]_{\text{bath}} = 0$  mM (five patches; 16 records at different voltages) and  $2$  mM (two patches; four records at different voltages), and in inside-out mode (four patches; eight observed records at different voltages), and no signs of two  $P_o$  modes were noted.

Thus, unlike M-channels in bullfrog sympathetic neurons, those in rat sympathetic neurons do not appear to show modal gating.

## DISCUSSION

Kinetic analysis of M-channel activity conducted in the present work suggests that this activity can be described by a five-state sequential model, where three closed states are separated by two open states (C-O-C-O-C). Although this model is almost certainly an oversimplification, and some states of the channel probably remained unresolved because of the limited resolution of the recording, it allowed us to satisfactorily simulate both steady-state and time-dependent activation and deactivation of M-channels.

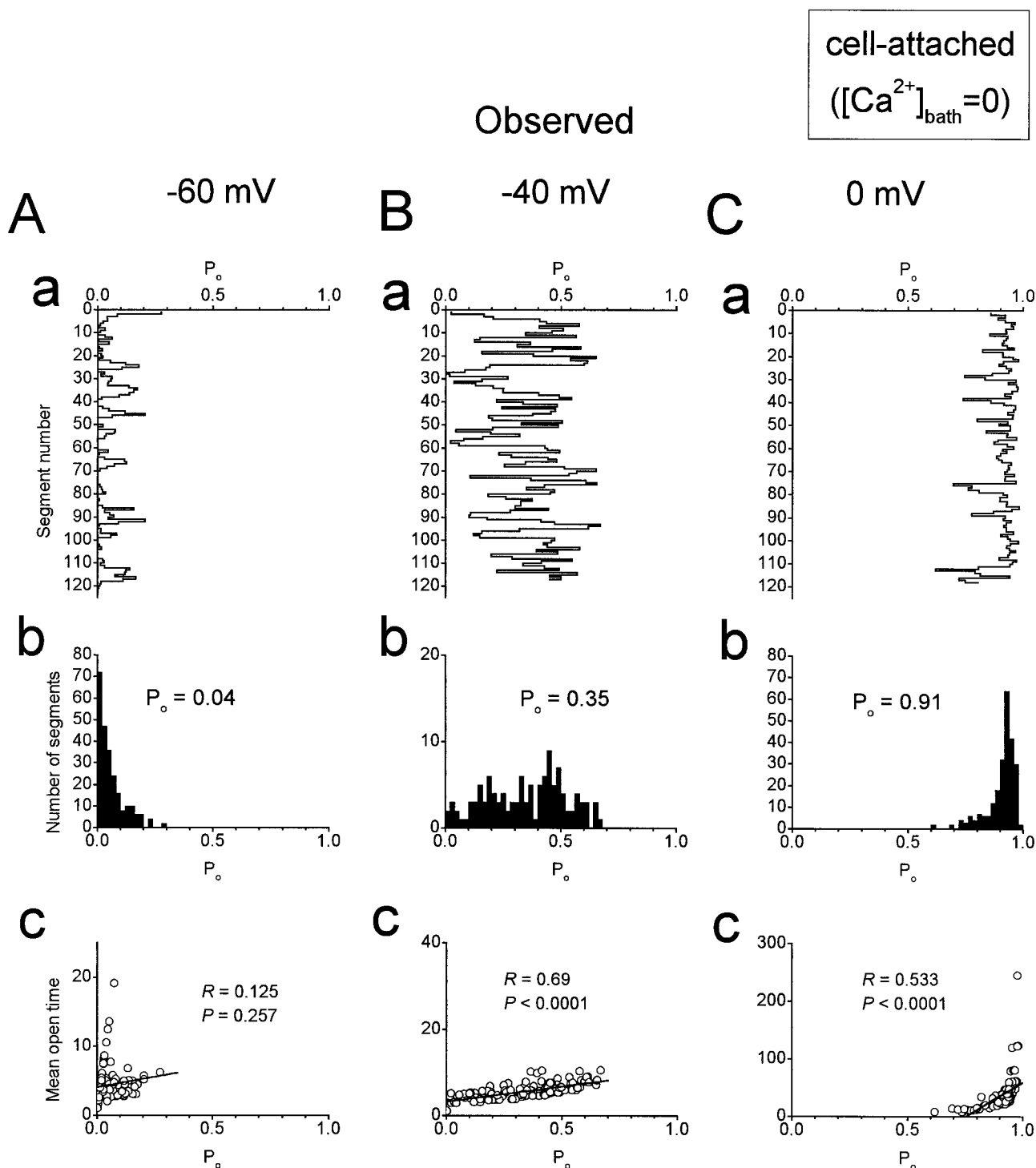


FIGURE 10 Runs analysis of M-channel activity does not show modal gating. (a) Runs analysis of  $P_o$  within 0.5-s segments, (b) distribution of  $P_o$  in segments, and (c) mean open time plotted against  $P_o$  in segments for the activity recorded in cell-attached mode in the absence of  $Ca^{2+}$  in the bath at  $-60$  mV (A),  $-40$  mV (B), and  $0$  mV (C). In C straight lines are linear regressions, with correlation coefficients ( $R$ ) and probability ( $P$ ) that the correlation was 0 indicated near each line. Data were obtained from the same cell-attached patch.

The linear (noncyclic) kinetic scheme, with no adjacent closed states, is consistent with such characteristic features of the M-current as lack of inactivation and absence of any delay in activation (for a review see Brown, 1988). The longest closed state ( $C_L$ ) in the activity is more than one

order longer than the other closed states. Because it shows a strong voltage dependence (see Fig. 5 Aa and Selyanko and Brown, 1993) and becomes dominant at near-threshold potentials for M-channel activation, it is probably in this state that the channel mainly dwells when it is deactivated at

potentials more negative than  $-60$  mV. Consistent with this, the concealment of this state as a result of patch excision into a  $\text{Ca}^{2+}$ -free solution is accompanied by a strong,  $\sim 20$ -mV negative shift in the activation curve for the M-channel (see Fig. 2). However, this shift cannot be explained entirely by the loss of  $\text{C}_L$ . Thus, in the absence of  $\text{C}_L$  the equilibrium in the kinetic scheme is shifted to the right, resulting in the larger contribution of long open times to the activity, which also contributed to high  $P_o$  at negative potentials. The reasons for its loss after the patch excision are not clear at the moment: it might (for instance) reflect the dissociation of an attached regulatory protein or a change in phosphorylation state.

Our C-O-C-O-C scheme is different from the one recently proposed for M-channels in bullfrog sympathetic neurons, namely O-C-C-C-O (Marrion, 1996). It should be pointed out that, although the M-channels in the two preparations have similar conductances and both are inhibited by muscarine and  $\text{Ca}_{in}^{2+}$  (Selyanko et al., 1992; Selyanko and Brown, 1996a,b; Marrion, 1993, 1996), they differ in some of their other properties. First, unlike the M-channels in frog sympathetic neurons (Marrion, 1993, 1996), those in the rat do not appear to show modal gating (present data). Second, muscarine inhibits both short and long channel openings in rat sympathetic neurons (Selyanko and Brown, 1993) but only long channel openings in frog sympathetic neurons (Marrion, 1993). Third,  $\text{Ca}_{in}^{2+}$  directly blocks the M-channels in rat sympathetic neurons (Selyanko and Brown, 1996a), and this effect is not mediated/reproduced by a phosphatase (Selyanko and Brown, 1996b), whereas in frog sympathetic neurons  $\text{Ca}_{in}^{2+}$ -induced inhibition is mediated by a  $\text{Ca}^{2+}$ -dependent phosphatase calcineurin (Marrion, 1996). Closer comparison between our kinetic data and those of Marrion (1996) is hampered by the fact that, in the latter work, the closed times and the burst structure were not analyzed; nor it has been shown whether the scheme O-C-C-C-O can be used to reconstruct the macroscopic M-current.

Recently, KCNQ2 and KCNQ3 subunits (related to the *KCNQ1* gene, which is partially responsible for cardiac QT syndrome; Yang et al., 1998), which are abundantly expressed in both the ganglia and the brain, have been proposed to contribute to the M-channel (Wang et al., 1998). Macroscopic currents carried by KCNQ2/KCNQ3 channels seem to be kinetically similar to the M-current (Yang et al., 1998; Wang et al., 1998; Schroeder et al., 1998). However, whether parameters of single KCNQ2/KCNQ3 channels are also similar to those of the M-channels, and whether they can be simulated within the proposed model, is yet to be established.

We thank Brenda Browning and Misbah Hall for tissue culture and Prof. David Colquhoun for his critical reading of the manuscript and helpful suggestions.

This work was supported by the Medical Research Council, U.K.

## REFERENCES

- Brown, D. A. 1988. M currents. *Ion Channels*. 1:55–94.
- Brown, D. A., and P. R. Adams. 1980. Muscarinic suppression of a novel voltage-sensitive  $\text{K}^+$  current in a vertebrate neurone. *Nature*. 283: 673–676.
- Colquhoun, D., and F. J. Sigworth. 1995. Fitting and statistical analysis of single-channel records. In *Single-Channel Recording*, 2nd Ed. B. Sakmann and E. Neher, editors. Plenum Press, New York. 483–587.
- Jackson, M. B., B. S. Wong, C. E. Morris, H. Lecar, and C. N. Christian. 1983. Successive openings of the same acetylcholine receptor channel are correlated in open time. *Biophys. J.* 42:109–114.
- Klemic, K. G., D. M. Durand, and S. W. Jones. 1998. Activation kinetics of the delayed rectifier potassium current of bullfrog sympathetic neurons. *J. Neurophysiol.* 79:2345–2357.
- Marrion, N. V. 1993. Selective reduction of one mode of M-channel gating by muscarine in sympathetic neurons. *Neuron*. 11:77–84.
- Marrion, N. V. 1996. Calcineurin regulates M channel modal gating in sympathetic neurons. *Neuron*. 16:163–173.
- Marrion, N. V. 1997. Control of M-current. *Annu. Rev. Physiol.* 59: 483–504.
- Rae, J., K. Cooper, P. Gates, and M. Watsky. 1991. Low access resistance perforated patch recordings using amphotericin B. *J. Neurosci. Methods*. 37:15–26.
- Schroeder, B. C., C. Kubisch, V. Stein, and T. J. Jentsch. 1998. Moderate loss of function of cyclic-AMP-modulated KCNQ2/KCNQ3  $\text{K}^+$  channels causes epilepsy. *Nature*. 396:687–690.
- Selyanko, A. A., and D. A. Brown. 1993. Effects of membrane potential and muscarine on potassium M-channel kinetics in rat sympathetic neurones. *J. Physiol. (Lond.)*. 472:711–724.
- Selyanko, A. A., and D. A. Brown. 1996a. Intracellular calcium directly inhibits potassium M channels in excised membrane patches from rat sympathetic neurons. *Neuron*. 16:151–162.
- Selyanko, A. A., and D. A. Brown. 1996b. Regulation of M-type potassium channels in mammalian sympathetic neurons: action of intracellular calcium on single channel currents. *Neuropharmacology*. 35:933–947.
- Selyanko, A. A., C. E. Stansfeld, and D. A. Brown. 1992. Closure of potassium M-channels by muscarinic acetylcholine-receptor stimulants requires a diffusible messenger. *Proc. R. Soc. Lond. B.* 3:147–159.
- Wang, H.-S., Z. Pan, B. S. Brown, R. S. Wymore, I. S. Cohen, J. E. Dixon, and D. McKinnon. 1998. KCNQ2 and KCNQ3 potassium channel subunits: molecular correlates of the M-channel. *Science*. 282: 1890–1893.
- Weiss, D. S., and K. L. Magleby. 1989. Gating scheme for single GABA-activated  $\text{Cl}^-$ -channels determined from stability plots, dwell-time distributions, and adjacent-interval durations. *J. Neurosci.* 9:1314–1324.
- Yang, W.-P., P. C. Levesque, W. A. Little, M. L. Conder, P. Ramakrishnan, M. G. Neubauer, and M. A. Blamnar. 1998. Functional expression of two KvLQT1-related potassium channels responsible for an inherited idiopathic epilepsy. *J. Biol. Chem.* 273:19419–19423.
- Zagotta, W. N., T. Hoshi, J. Dittman, and R. W. Aldrich. 1994. *Shaker* potassium channel gating. III. Evaluation of kinetic models for activation. *J. Gen. Physiol.* 103:321–362.